Spin–orbit splitting-dependent quadratic electro-optic effect in InGaN/GaN quantum wells

2007 J. Phys.: Condens. Matter 19 236234

(http://iopscience.iop.org/0953-8984/19/23/236234)

IOP PUBLISHING JOURNAL OF PHYSICS: CONDENSED MATTER

J. Phys.: Condens. Matter **19** (2007) 236234 (12pp) doi:10.1088/0953-8984/19/23/236234

Spin–orbit splitting-dependent quadratic electro-optic effect in InGaN/GaN quantum wells

Youqing Yu[1], **Fei Gao**[1] **and Guiguang Xiong**[1,2,3]

[1] Department of Physics, Wuhan University, Wuhan 430072, People's Republic of China
[2] Key Laboratory of acoustic and Photonic Materials and Devices, Ministry of Education, 430072, People's Republic of China

Received 24 October 2006, in final form 26 March 2007
Published 17 May 2007
Online at stacks.iop.org/JPhysCM/19/236234

Abstract

Taking account of the contribution of spin–orbit splitting, the energy band of GaN/InGaN quantum wells (QWs) has been calculated. For the quadratic electro-optic effect (QEOE), the resonant third-order nonlinear optical susceptibility due to the interband transition of the mode, whose polarization is parallel to the [0 0 1] direction of the QWs, has been analysed as a function of the well width and the concentration of In.

1. Introduction

Recently, GaN-based semiconductor material and devices have caused great interest in people because of their many advantages, for example wide band gap, high electron saturated drift velocity and great thermal conductivity [1–5]. Among them, the quantum-confined structures, including quantum wells, wires and dots, are very active, in which the carriers are confined in one, two and three dimensions correspondingly. The discrete energy levels, resulting from the quantum confinement effect, cause many unique physical properties. Compared to bulk material, the nonlinear optical effects in GaN/InGaN quantum wells are stronger. Although there have been some experimental reports [6–9], it is important and significant to calculate the third-order nonlinear optical susceptibility of the GaN-based QWs.

As we all know, there are two kinds of transition processes occurring in semiconductor quantum wells. Many studies of conduction intraband transitions (the transition between two different subbands in the conduction band) have been reported [10, 11]. However, to light-emitting diodes (LEDs) and laser diodes (LDs), intersubband transitions (the transitions between a valence subband and a conduction subband) are more important. Different from GaAs-based quantum wells [12, 13], the spin–orbit split-off energy of GaN/InGaN QWs is very small and similar to the energy difference between valence subbands. So, for GaN/InGaN QWs, the contribution of spin–orbit splitting cannot be neglected in the calculation of the valence band structure and nonlinear optical susceptibility due to intersubband transitions. In this paper, to understand the impacts of structure and material on nonlinear optical effects, the third-order nonlinear optical susceptibility due to the intersubband transition for the parallel mode in the

[3] Author to whom any correspondence should be addressed.

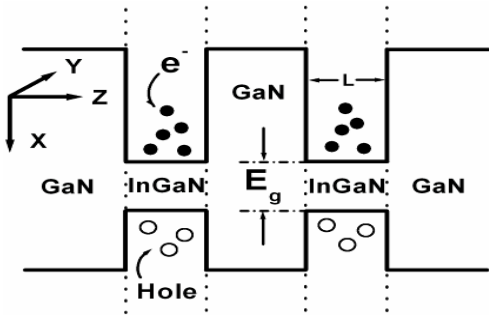

Figure 1. The structure of GaN/InGaN QWs.

GaN/InGaN quantum wells, including the contribution of the spin–orbit splitting, has been calculated as a function of the well width and the concentration of the material In.

2. Model and theory

The structure of the GaN/InGaN QWs used in this paper is shown in figure 1. Because of the implantation of the material In, the energy gap of InGaN is smaller than GaN and thus the InGaN layers form potential wells. Since the potential barrier GaN layer between two neighbouring wells is wide enough, the wavefunctions in the wells will not be overlapped and the multiple quantum wells can be treated as a single quantum well (QW).

Using the approximation of effective mass [14, 15], the wavefunction near the Γ point in the first Brillouin zone of the QW can be expanded as:

$$\Psi(\mathbf{r}) = \sum_{\mathrm{n}} U_{\mathrm{n}}(\mathbf{r}) F_{\mathrm{n}}(\mathbf{r}). \tag{1}$$

Here $F_{\mathrm{n}}(\mathbf{r})$ is the slowly-varying envelope function and $U_{\mathrm{n}}(\mathbf{r})$ is the Bloch function. For the holes in the valence band, $U_{\mathrm{n}}(\mathbf{r})$ corresponds to six band-edge wavefunctions, $|v_{\mathrm{n}}\rangle$ ($n = 1, 2, 3, \ldots, 6$). For the electrons in the conduction band, $U_i(\mathbf{r}) = |C\rangle$, and $|C\rangle$ is the ground-state wavefunction of electrons. In this way, the effective mass equations of the electrons and holes can be obtained.

With the contribution of spin–orbit splitting, the holes of the valence band in the GaN/InGaN QW are divided into three types: (i) the heavy holes, which denote that the value of $\partial^2 E/\partial^2 k$ and the corresponding effective masses are large; (ii) the light holes, which denote that the values of $\partial^2 E/\partial^2 k$ and the corresponding effective masses are small; (iii) the spin–orbit split-off holes, which are generated by the interaction between the magnetic torque from the spin of valence electrons and the magnetic field from the orbits of other valence electrons. Considering the direction of spin, there are three two-fold degenerated energy levels at the top of the valence band. Thus the Hamiltonian of the valence band can be written as the 6×6 Luttinger–Kohn matrix [16, 17]:

$$H_0(k_x, k_y, k_z) = \begin{bmatrix} A_+ & C & \frac{\mathrm{i}}{\sqrt{2}}C & -\mathrm{i}\sqrt{2}B & B & 0 \\ C^* & A_- & -\frac{\mathrm{i}}{\sqrt{2}}(A_+ - A_-) & \mathrm{i}\sqrt{\frac{3}{2}}C & 0 & b \\ -\frac{\mathrm{i}}{\sqrt{2}}C^* & \frac{\mathrm{i}}{\sqrt{2}}(A_+ - A_-) & -\Delta + \frac{1}{2}(A_+ + A_-) & 0 & \mathrm{i}\sqrt{\frac{3}{2}}C & \mathrm{i}\sqrt{2}B \\ \mathrm{i}\sqrt{2}B^* & -\mathrm{i}\sqrt{\frac{3}{2}}C^* & 0 & -\Delta + \frac{1}{2}(A_+ + A_-) & \frac{\mathrm{i}}{\sqrt{2}}(A_+ - A_-) & \frac{\mathrm{i}}{\sqrt{2}}C \\ B^* & 0 & -\mathrm{i}\sqrt{\frac{3}{2}}C^* & -\frac{\mathrm{i}}{\sqrt{2}}(A_+ - A_-) & A_- & -C \\ 0 & B^* & -\mathrm{i}\sqrt{2}B^* & -\frac{\mathrm{i}}{\sqrt{2}}C^* & -C^* & A_+ \end{bmatrix} \tag{2}$$

where Δ denotes the split of the spin–orbit coupling. A_+, A_-, B and C have the forms:

$$\begin{aligned} A_\pm &= -\frac{\hbar^2}{2m_0}[(k_x^2+k_y^2)(\gamma_1 \pm \gamma_2) + k_z^2(\gamma_1 \mp 2\gamma_2)] \\ B &= -\frac{\sqrt{3}\hbar^2}{2m_0}[\gamma_2(k_x^2-k_y^2) - \mathrm{i}2\gamma_3 k_x k_y] \\ C &= \frac{\sqrt{3}\hbar^2}{m_0}\gamma_3(\mathrm{i}k_x + k_y)k_z \end{aligned} \tag{3}$$

where γ_1, γ_2 and γ_3 are Luttinger parameters. Since there is no confinement in the directions of x and y, the method of separation of variables can be used and the envelope functions of the holes can be rewritten as:

$$F_\mathrm{v}(k_x, k_y, z) = \frac{1}{\sqrt{L_x L_y}}\mathrm{e}^{\mathrm{i}(k_x x + k_y y)} f_\mathrm{v}(z); \tag{4}$$

here L_x and L_y are the normalized constants, which denote the length of the QW in the directions of x and y, respectively.

Thus the effective mass equation for the valence band is:

$$H_0(k_x, k_y, z)[f_m(z)] = E(k_x, k_y, z)[f_m(z)], \tag{5}$$

where $m = \mathrm{HH}\uparrow, \mathrm{LH}\uparrow, \mathrm{SO}\uparrow, \mathrm{SO}\downarrow, \mathrm{LH}\downarrow, \mathrm{HH}\downarrow$ denotes the terms for heavy holes, light holes and the spin–orbit split-off holes with opposite spins. Near the top of the valence band, $f_m(z)$ can be expanded as:

$$f_m(z) = \sqrt{\frac{2}{L}}\sum_{n=1}^{N} c_\mathrm{n}^m \sin\frac{n\pi z}{L}. \tag{6}$$

As shown in figure 1, L denotes the width of the QW. Combining (5) with (6), the eigenvalue equation can be obtained as:

$$[H][C^m] = E[C^m], \tag{7}$$

where $[H]$ is a $6N \times 6N$ matrix obtained from (2) and the eigenfunction is:

$$[C^m] = (C_{HH\uparrow}, C_{LH\uparrow}, C_{SO\uparrow}, C_{SO\downarrow}, C_{LH\downarrow}, C_{HH\downarrow})^\mathrm{T}, \tag{8}$$

$$C_i = (C_1^i, C_2^i, C_3^i \ldots C_N^i)^\mathrm{T}. \tag{9}$$

Thus, by solving the eigenvalue problem, the energy structure of the holes near the top of the valence band can be obtained.

As for the electrons near the bottom of the conduction band, it is simpler than the situation for holes. After the effective mass equation is given, the method of separation of variables can also be used on the slow envelope wavefunction of the electrons, since the QW forms discrete quantized energy levels in the direction of z and the electrons are confined only in the z direction. Setting the energy level at the top of the valence band to be zero, the wavefunction and the energy at the Γ point for electrons at the bottom of the conduction band are:

$$f_\mathrm{n}(k_x, k_y, z) = \frac{1}{\sqrt{L_x L_y}}\exp[\mathrm{i}(k_x x + k_y y)]\sqrt{\frac{2}{L}}\sin\frac{n\pi z}{L}, \tag{10}$$

$$E = E_\mathrm{g} + \frac{\hbar^2(k_x^2+k_y^2)}{2m_\mathrm{e}^*} + \frac{\hbar^2 n^2\pi^2}{2m_\mathrm{e}^* L^2}, \tag{11}$$

here E_g is the energy gap, and m_e^* is the effective mass of the electrons.

According to the selection rules of the transition between the valence and conduction bands, the transition between the valence band and the conduction subband can exist only when $\Delta n = 0$. Considering that the envelope function varies slowly, the element of the transition matrix, whose quantum number is n, is:

$$\langle r_p \rangle_{\mathrm{n}} = \int \Psi_{\mathrm{c}}^*(\mathbf{r}) r_p \Psi_{\mathrm{v}}(\mathbf{r})\, \mathrm{d}^3\mathbf{r} = \sum_{i=1}^{6} \langle c|r_p|v_i\rangle \int f_{\mathrm{c}}^*(z) f_{\mathrm{v}}^i(z)\, \mathrm{d}z = \sum_{i=1}^{6} \langle c|r_p|v_i\rangle C_{\mathrm{n}}^i. \tag{12}$$

Note that [18]:

$$\langle c|r_p|v_i\rangle = \langle e, j'|r_p|r_q, j\rangle = \frac{\hbar}{E_{\mathrm{c}} - E_{\mathrm{v}}} \sqrt{\frac{E_{\mathrm{g}}(E_{\mathrm{g}} + \Delta)}{2m_{\mathrm{e}}^*(E_{\mathrm{g}} + \frac{2}{3}\Delta)}} \delta_{j,j'}\delta_{p,q}. \tag{13}$$

In (12) and (13), $r_{p,q=1,2,3} = x, y, z$, $\delta_{j,j'}\delta_{p,q}$ denotes that there is no transition between different directions and different spins. The band-edge wavefunctions of the holes ($|3/2, \pm 3/2\rangle$, $|3/2, \pm 1/2\rangle$, $|1/2, \pm 1/2\rangle$) are shown in [12]. Taking them into (13), and setting

$$\frac{\hbar}{E_{\mathrm{c}} - E_{\mathrm{v}}} \sqrt{\frac{E_{\mathrm{g}}(E_{\mathrm{g}} + \Delta)}{2m_{\mathrm{e}}^*(E_{\mathrm{g}} + \frac{2}{3}\Delta)}} = \Omega, \tag{14}$$

the matrix element of the dipole transition in the z direction between the nth subband of the valence band and the nth subband of the conduction band can be written as:

$$z_{e\uparrow,v} = \left(-\mathrm{i}\sqrt{\frac{2}{3}} C_{\mathrm{n}}^2 + \frac{C_{\mathrm{n}}^3}{\sqrt{3}}\right)\Omega,\ z_{e\downarrow,v} = \left(\frac{\mathrm{i}C_{\mathrm{n}}^4}{\sqrt{3}} + \sqrt{\frac{2}{3}} C_{\mathrm{n}}^5\right)\Omega. \tag{15}$$

So far, the energy structure and the wavefunctions of holes near the top of the valence band and electrons near the bottom of the conduction band can be obtained. If we know the expression of the third-order nonlinear optical susceptibility, it is easy to get the impacts of the structure and the material on it.

The original expression for third-order nonlinear optical susceptibility is [19]:

$$\chi^{(3)}_{\mu\alpha\beta\gamma}(-\omega_\sigma; \omega_1, \omega_2, \omega_3) = \frac{-e^4}{6\omega_\sigma\omega_1\omega_2\omega_3\hbar^3 m^4 V} \sum_p \sum_{a,b,c,d} \sum_k f(a,k) \times \frac{p_{ab}^\mu p_{bc}^\alpha p_{cd}^\beta p_{da}^\gamma}{(\Omega_{ba} - \omega_1 - \omega_2 - \omega_3)(\Omega_{ca} - \omega_1 - \omega_2)(\Omega_{da} - \omega_1)} \tag{16}$$

where ω_1, ω_2, ω_3 are the frequencies of the incident radiation and α, β, γ are their respective polarizations, and p represents a dipole matrix element. The polarization of the response is μ and its frequency is $\omega_\sigma = \omega_1 + \omega_2 + \omega_3$. $\sum_{a,b,c,d}$ represents a summation over superlattice bands, and $\sum_k$ represents a summation over the Brillouin zone. $f(a,k)$ is the occupation number of states in the ground state, and $\Omega_{ba} = (E_b - E_a)/\hbar - \mathrm{i}\gamma_{ba}$. $\sum_p$ represents a sum over permutations of the pairs $(\mu, -\omega_\sigma)$, (α, ω_1), $(\beta, \omega_2)(\gamma, \omega_3)$. In this paper, the dc field can be considered as a coherent superposition of the photon with zero frequency. The dc-Kerr effect and the electron-absorption process can be described by the third-order nonlinear susceptibility: $\chi^{(3)}_{\mathrm{QEOE}}(\omega) = \mathrm{Re}\,\chi^{(3)}(-\omega, 0, 0, \omega)$, $\chi^{(3)}_{\mathrm{EA}}(\omega) = \mathrm{Im}\,\chi^{(3)}(-\omega, 0, 0, \omega)$. For the mode parallel to the [0 0 1] direction of the QW, the third-order nonlinear optical susceptibility $\chi^{(3)}(-\omega, 0, 0, \omega)$, due to the transitions from the valence band to the conduction band, can be obtained from formula (16), shown as follows [12, 13]:

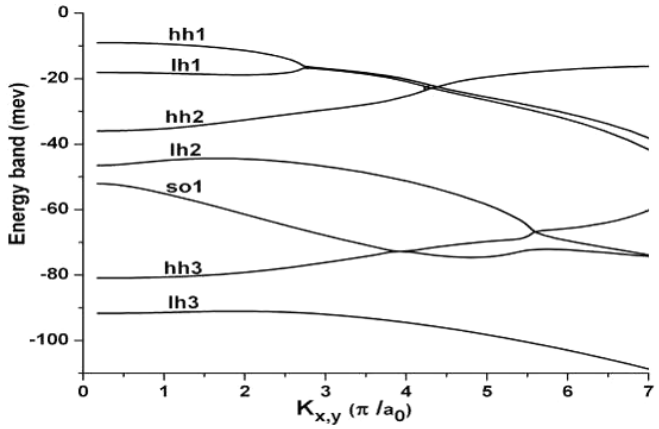

Figure 2. The energy of the holes as a function of $\vec{k}$ vertical to the z-direction of the MQWs.

$$\chi^{(3)}(-\omega,0,0,\omega) = \frac{e}{L}\left(\frac{e}{2\hbar}\right)^3 \int \frac{\mathrm{d}k^2}{(2\pi)^2} \times \sum_{v,v'=HH,LH,SO} \langle c|z|v\rangle\langle v|z|c'\rangle\langle c'|z|v'\rangle\langle v'|z|c\rangle(\rho_c^0 - \rho_v^0)\frac{1}{\omega - \mu_{c',v}} \times \left(\frac{1}{\omega + \mu_{v,v'}^*} \times \frac{1}{\omega - \mu_{c,v}} + \frac{1}{\omega + \mu_{c,c'}^*} \times \frac{1}{\omega - \mu_{c',v'}}\right). \tag{17}$$

The suffixes c, c' denote the two-fold degenerated state with opposite spins in the conduction band and v, v' denote one of the three two-fold degenerate states with opposite spins in the valence band. ρ_c^0 and ρ_v^0 are the quasi-Fermi energies, $\rho_c^0 = 0.15$ eV and $\rho_v^0 = 0.05$ eV. $\mu_{cv}(k)$ is defined as:

$$\mu_{cv}(k) = \frac{E_c(k) - E_v(k)}{\hbar} - \mathrm{i}\gamma_{cv}, \tag{18}$$

where $E_c(k)$ and $E_v(k)$ are the energies of the electrons in the conduction band and the holes in the valence band, $\gamma_{cv} = 1/\tau_{cv}$, $\tau_{cv} = (\tau_{cc} + \tau_{vv})/2$, and τ_{cc} and τ_{vv} are the relaxation times of the electrons and holes and can be assumed to be $\tau_{cc} = \tau_{vv} = 10^{-13}$ s.

3. Results and discussions

Setting the concentration of In to be 0.05, the parameters of the potential well material InGaN are given in table 1 [20].

After defining the energy at the top of the valence band to be zero, the energy structure of the holes near the top of the valence band is shown in figure 2, while the width of the QW is set as 7.0 nm and the concentration of In as 0.05.

At room temperature, the electrons and holes in the QW are distributed mainly near the bottom of the conduction band and the top of the valence band, respectively. Most of the carriers are near the state $n = 1, \vec{k} = 0$. According to the rules of selection, the intersubband transition can be described as the transition from the HH1, LH1 or SO1 valence subband to the first conduction subband. Thus the n in (15) is equal to 1. Taking the wavefunctions into (17), the modulus, real and imaginary parts of $\chi^{(3)}_{\mathrm{QEOE}}$ can be obtained, shown in figure 3.

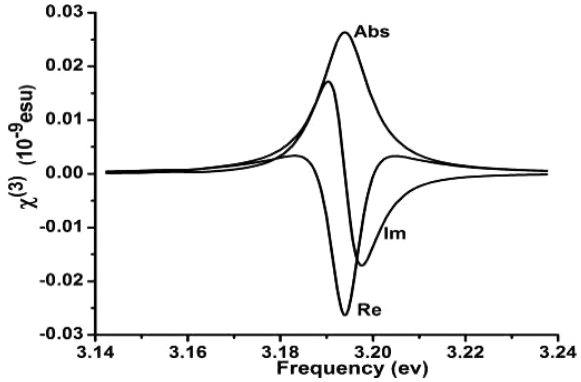

Figure 3. The modulus, real part and imaginary part of $\chi^{(3)}_{\mathrm{QEOE}}$.

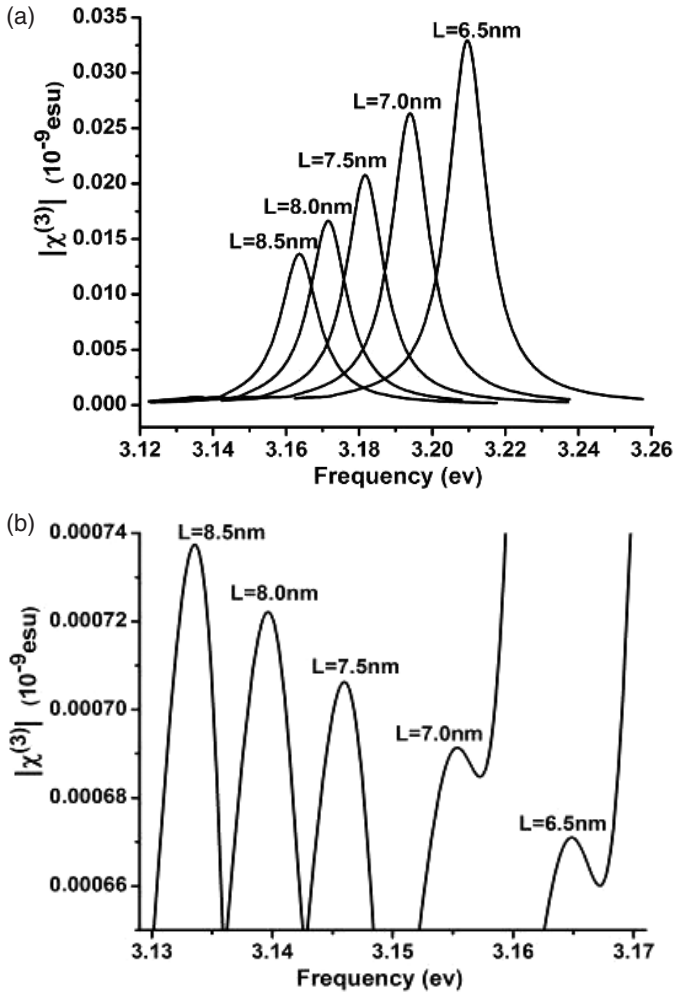

Figure 4. The modulus of $\chi^{(3)}_{\mathrm{QEOE}}$ with different well width.

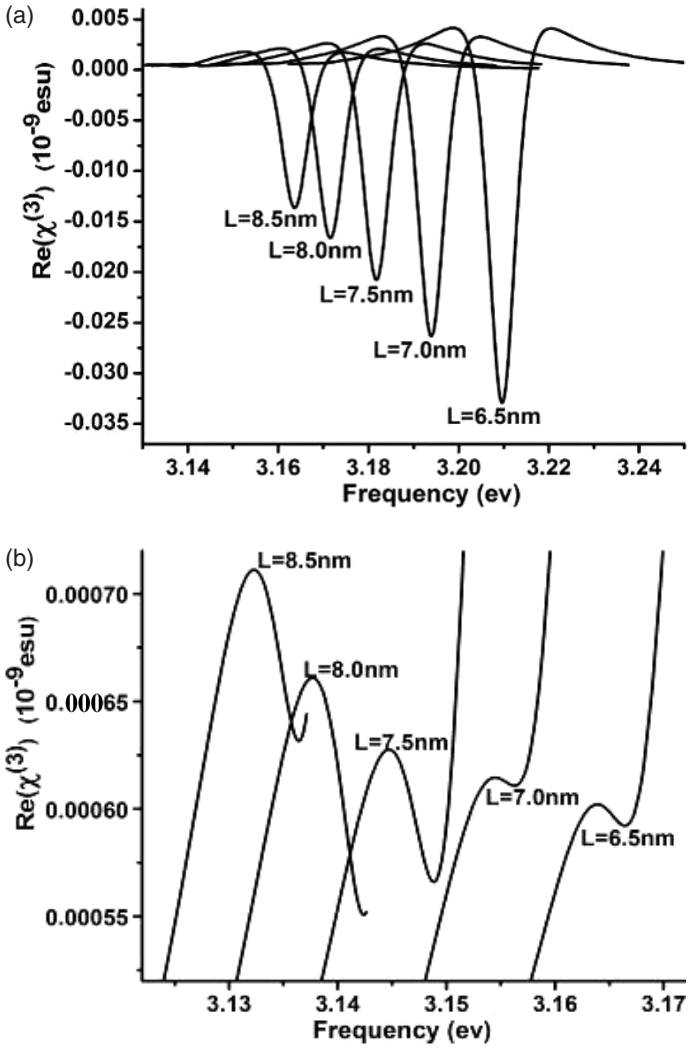

Figure 5. The real part of $\chi^{(3)}_{\mathrm{QEOE}}$ with different well width.

Table 1. The parameters of InGaN that are used.

Parameters	$In_{0.05}Ga_{0.95}N$
Length of primitive cell: a_0 (Å)	4.50
Forbidden gap: E_g (eV)	3.088 55
Effective mass: m_e^*	0.148 5
Luttinger parameters:	
γ_1	2.722 5
γ_2	0.775 5
γ_3	1.126 5

From (8), (9) and (15), it can easily be seen that for the mode, whose polarization is parallel to the [0 0 1] direction of the QW, the HH1 state has no contribution to the transition process. From figure 3, it seems that there is only one peak in each one of the three curves. But this

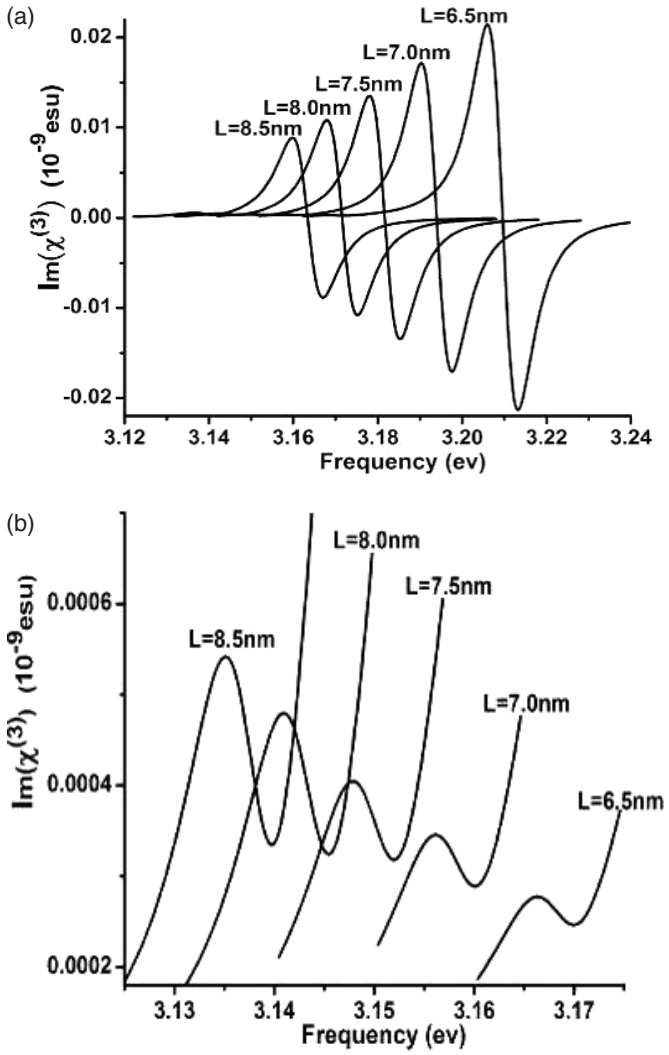

Figure 6. The imaginary part of $\chi^{(3)}_{\mathrm{QEOE}}$ with different well width.

is not true. In fact, near the frequency of 3.15 eV, there is another peak in each curve, which is too tiny to be seen. The great difference between the values of the two peaks results from different transition probabilities. Since the tiny peak is due to the transition from the first light hole valence subband LH1 to the first conduction subband e1 while the large peak is due to the transition from the first spin–orbit split-off hole valence subband SO1 to e1, the great difference shows that the mode with polarization parallel to the [0 0 1] direction of the GaN/InGaN QW is more sensitive to the transition from SO1 than LH1 to e1. From this point, some spin-dependent dynamic research can be performed in the future.

Furthermore, to understand the impacts of the material and structure of the QW on the nonlinear optical effects, the modulus, real and imaginary parts are given as functions of the well width and the concentration of In, respectively.

As the concentration of In is fixed at 0.05, the modulus, real and imaginary parts of $\chi^{(3)}_{\mathrm{QEOE}}$ are shown in figures 4–6 with varying well width from 6.5 to 8.5 nm. There are two peaks

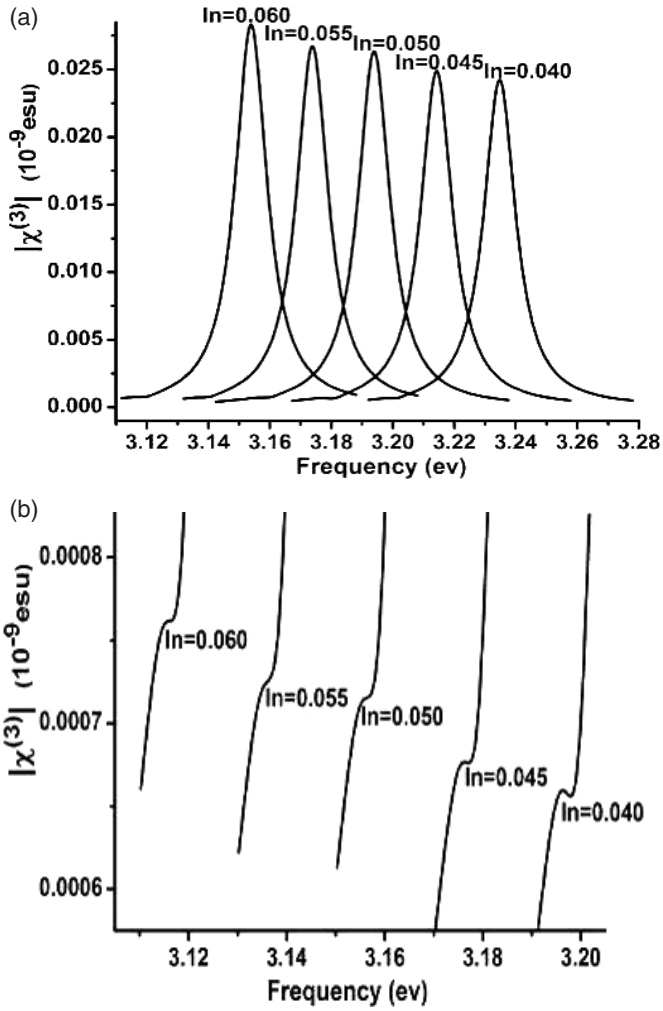

Figure 7. The modulus of $\chi^{(3)}_{\mathrm{QEOE}}$ with different concentrations of In.

in each curve. However, the tiny peak near the low frequency is too small to be seen, which is smaller than that near the high frequency by over one order of magnitude. So, with the frequency confined from 3.13 to 3.17 eV, the tiny peaks, due to the transition from LH1 to e1, are magnified in figures 4(b), 5(b) and 6(b). From both (a) and (b) of figures 4–6, with an increase in well width, the position of the peaks generates red-shift. This indicates that the energy difference between LH1 or SO1 and e1 decreases as the well width increases. On the other hand, the value of the peaks, which are due to the transition from SO1 to e1, decreases with an increase in well width. Because of the great difference in the value of the two peaks, it can be seen that the QEOE will increase with an decrease in well width. This indicates that with the increase in well width, the quantum confinement effect and correspondingly the third-order nonlinear optical effect will become weaker.

In contrast, from figures 4(b), 5(b) and 6(b), the value of the peaks, due to the transition from LH1 to e1, increases as the well width increases. This is an interesting phenomenon and we think it results from the following reasons. In the GaN/InGaN QW, the discrete quantized

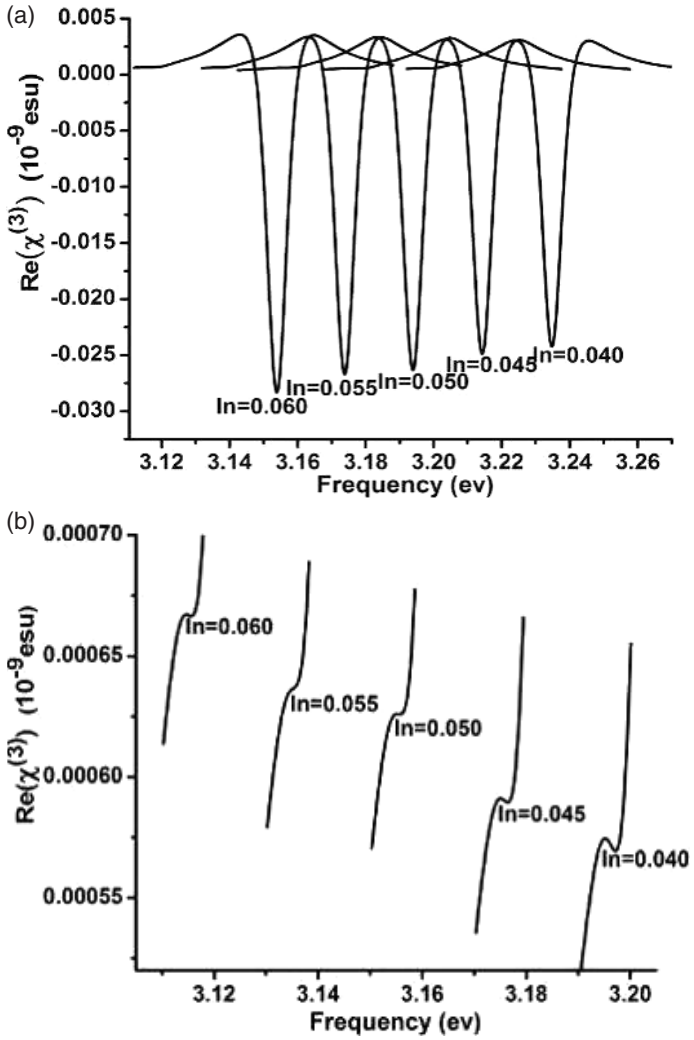

Figure 8. The real part of $\chi^{(3)}_{\mathrm{QEOE}}$ with different concentrations of In.

energy levels are formed in the z direction, while the particles with effective masses move freely in the x–y plane. For the holes of the valence band, the motions in the x, y and z directions are coupled mutually and every valence subband has a contribution for HH, LH and SO. Only at $k_x = k_y = 0$, the wavefunction of each subband tends to that of the corresponding hole state. The GaN/InGaN QW is Type I QW and the carriers are distributed mainly near the Γ point ($k = 0$). However, in a real situation, the wavevectors parallel to the layer are not zero ($k_x \neq 0, k_y \neq 0$), which results in the coupling of HH and LH. This can be seen from figure 2, in which the curvature of the LH1 subband near the frequency of $2.5\pi/a_0$ becomes positive. The HH1 holes have much effect on the transition process from LH1 to e1 and the influence becomes greater with decreasing well width. Since HH1 has no contribution to the third-order nonlinear susceptibility of the mode with the polarization parallel to the [0 0 1] direction of the QW, the value of the peaks due to the transition from LH1 to e1 decreases with decreasing well width.

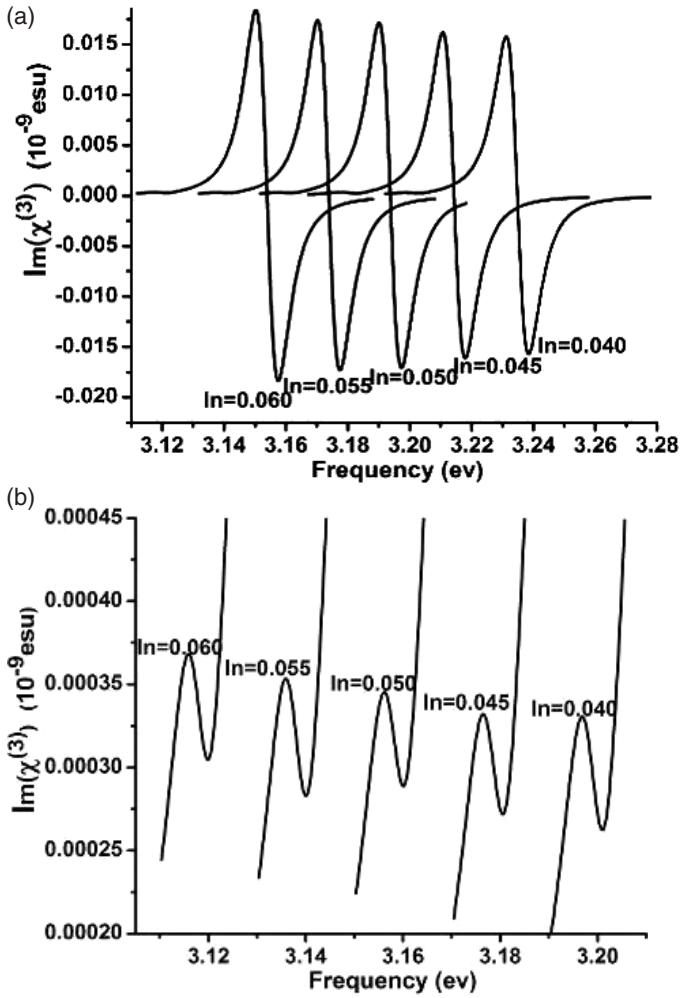

Figure 9. The imaginary part of $\chi^{(3)}_{\mathrm{QEOE}}$ with different concentrations of In.

In addition, setting the width of the potential well to be 7 nm, the modulus, real and imaginary parts are shown with varying concentrations of the semiconductor material In.

From figures 7 to 9, it can be seen easily that, with an increase in the concentration of In, the peaks generate red-shift and become bigger. The red-shift indicates that the energy difference between LH1 or SO1 and e1 becomes small as the concentration of In increases. In addition, the increase in the peak values shows that, within a certain range, the quantum confinement effect, and correspondingly the third-order nonlinear optical effects, will become stronger with an increase in the concentration of In.

4. Conclusions

Including the contribution of the spin–orbit splitting, the energy band structure has been calculated. Then the third-order nonlinear optical susceptibility for the quadratic electro-optic effect due to the intersubband transition of the mode, whose polarization is parallel to the [0 0 1] direction of the QW, has been analysed. The results show that the spin–orbit split-

off holes contribute more to the susceptibility than the light holes. With the increase in the well width and the concentration of In, the energy difference between LH1 or SO1 and e1 becomes smaller and the nonlinear susceptibility generates red-shift correspondingly. On the other hand, with the increase in the well width, the values of the peaks due to the transition from SO1 to e1 decrease while those due to LH1 to e1 increase, which results from the strong coupling between HH1 and LH1. With the increase in the concentration of In, the values of the peaks due to the transitions from both LH1 and SO1 to e1 increase. The results are significant for studying the competition between different modes in the QW and are useful for designing new semiconductor QW optoelectronic devices.

Acknowledgment

This work was supported financially by the Natural Science Foundation of China (grant number 10534030).

References

[1] Tachibana K, Someya T, Ishida S and Arakawa Y 2000 *Appl. Phys. Lett.* **76** 3212
[2] Martinez-Guerrero E, Chabuel F, Daudin B, Rouviere J L and Mariette H 2002 *Appl. Phys. Lett.* **81** 5117
[3] Arakawa Y and Sakaki H 1982 *Appl. Phys. Lett.* **40** 939
[4] Yariv A 1988 *Appl. Phys. Lett.* **52** 88
[5] Shen B, Someya T, Moriwali O and Arakawa Y 2000 *Physica* E **7** 939
[6] Feltin E, Simeonov D, Carlin J-F, Butté R and Grandjean N 2007 *Appl. Phys. Lett.* **90** 021905
[7] Kundys D O, Wells J-P R, Andreev A D, Hashemizadeh S A, Wang T, Parbrook P J, Fox A M, Mowbray D J and Skolnick M S 2006 *Phys. Rev.* B **73** 165309
[8] Omae K, Kawakami Y, Fujita S, Narukawa Y and Mukai T 2003 *Phys. Rev.* B **68** 085303
[9] Özgür Ü and Everitt H O 2003 *Phys. Rev.* B **67** 155308
[10] Bernandini F and Fiorentini V 2001 *Phys. Rev.* B **64** 5207
[11] Liu J, Bai Y and Xiong G 2004 *Physica* E **23** 70
[12] Takahashi Y, Neogi A and Kawaguchi H 1998 *IEEE J. Quantum Electron.* **34** 1660
[13] Takahashi Y and Kawaguchi H 2000 *IEEE. J. Quantum Electron.* **36** 864
[14] Luttinger J M and Kohn W 1955 *Phys. Rev.* **97** 869
[15] Luttinger J M 1955 *Phys. Rev.* **102** 1030
[16] Singh J 1993 *Physics of Semiconductors and Their Heterostructures* (New York: McGraw-Hill)
[17] Ivchenko E L and Pikus G 1995 *Superlattices and Other Heterostructures* (Berlin: Springer)
[18] Kane E O 1957 *J. Phys. Chem. Solids* **1** 249
[19] Shaw M J, Ninno D, Adderley B M and Jaros M 1992 *Phys. Rev.* B **45** 11031
[20] Vurgaftman I, Meyer J R and Ram-Mohan L R 2001 *J. Appl. Phys.* **89** 5815